In vivo imaging of *Drosophila melanogaster* pupae with mesoscopic fluorescence tomography

Claudio Vinegoni[1,2,5], Chrysoula Pitsouli[3,5], Daniel Razansky[1,4,5], Norbert Perrimon[3] & Vasilis Ntziachristos[1,4]

We report a technique for fluorescence tomography that operates beyond the penetration limits of tissue-sectioning fluorescence microscopy. The method uses multi-projection illumination and photon transport description in opaque tissues. We demonstrate whole-body three-dimensional visualization of the morphogenesis of GFP-expressing salivary glands and wing imaginal discs in living *Drosophila melanogaster* pupae *in vivo* and over time.

Progress in the biological sciences has often been associated with the evolution of optical imaging and the corresponding capacity to identify spatially distributed biomarkers. At the organ and organism level, optical biological imaging has traditionally focused on studying thin sections of dead specimens that produce minimal photon scattering. To study living biological specimens in unperturbed environments and over time, advances in optical microscopy for *in vivo* imaging have focused on physical methods to reject scattered photons from thick tissues[1–4]. These methods can resolve certain photon-tissue and photochemical interactions within well-confined unit volumes in tissues but are only suitable for operation at object sizes (depths) that are smaller than one transport mean free path-length (MFPL; the distance a photon travels before it is scattered or absorbed).

To reach deeper in tissues, macroscopic optical imaging by contrast relies on the use of highly scattered photons and is now applied to structures that are generally larger than several MFPL. Although simple photography is occasionally considered for *in vivo* optical imaging[5], optical macroscopy in its more advanced form illuminates the sample under investigation at multiple projections and uses mathematical models of photon propagation in tissues to reconstruct the underlying imaging contrast, albeit with much lower resolution than in microscopy[6]. In contrast to the terminology that applies to microscopic three-dimensional tissue-sectioning imaging, 'tomography' and 'reconstruction' here implies the formulation of a mathematical inverse problem, whose algebraic solution (minimization) yields the reconstructed images[7], in analogy to methods used in X-ray computed tomography (CT), single-photon emission tomography or positron emission tomography.

Currently, neither microscopic nor macroscopic reconstruction approaches are suitable for *in vivo* or 'longitudinal' visualization of developing insects, animal embryos or small-animal extremities. For whole-body visualization of those targets, a new imaging approach is required that will account for the correct photon propagation regime in mesoscopic-scale objects. Here we consider a mesoscopic imaging approach that could accelerate studies of morphogenesis and allow us to follow development in response to stimuli, including environmental agents, chemicals and drugs, on the same animal over time, with resolution higher than what is achieved by reconstruction methods developed for macroscopic imaging and penetration depths that can extend beyond the limits of presently available microscopy approaches. Previously, others[8] had considered optical projection tomography (OPT) for imaging fixed embryos; this technique and others[9], however, have only been used post-mortem on embryos that were chemically treated to reduce scattering and to increase a specimen's transparency, and are therefore not appropriate for live *in vivo* imaging.

Here we report the use of the Fermi simplification to the Fokker-Planck solution of photon transport theory[10], which operates in strongly forward-scattering regimes, as typical for photon scattering in tissues. This is different from what happens in OPT, where the sample is transparent and the photons are considered traveling without any scattering, making OPT an optical equivalent of X-ray CT scanning (reconstructions of three-dimensional images of the attenuation coefficient or the emission distribution are therefore obtained by back-propagating the photons using an inverse Radon transform). Using this theoretical model and a modified microscopic experimental setup we constructed a tomographic scheme for fluorescence tomography of *D. melanogaster* in prepupal and early pupal stages. We selected *D. melanogaster* because of its importance as a model organism and the ease with which one can generate tissue-specific GFP-expressing flies. Although *D. melanogaster* development is being studied extensively at the embryonic and larval stages because of the availability of many mutants and genetic tools, there is a lack of adequate techniques to monitor changes during pupal stages.

The opaque pupa undergoes extensive tissue remodeling before it becomes an adult fly. Although conventional epifluorescence microscopy[11,12] or confocal imaging of relatively superficially located cell

[1]Center for Molecular Imaging Research, Massachusetts General Hospital and Harvard Medical School, Building 149, 13th Street, Charlestown, Massachusetts 02129, USA. [2]Center for System Biology, Massachusetts General Hospital and Harvard Medical School, Richard B. Simches Research Center, 185 Cambridge Street, Boston, Massachusetts 02114, USA. [3]Department of Genetics, Harvard Medical School and Howard Hughes Medical Institute, 77 Avenue Louis Pasteur, Boston, Massachusetts 02115, USA. [4]Institute for Biological and Medical Imaging, Technical University of Munich and Helmholtz Center Munich, Ingolstädter Landstraße 1, D-85764 Neuherberg, Germany. [5]These authors contributed equally to this work. Correspondence should be addressed to C.V. (cvinegoni@mgh.harvard.edu).

RECEIVED 17 SEPTEMBER; ACCEPTED 19 NOVEMBER; PUBLISHED ONLINE 9 DECEMBER 2007; DOI:10.1038/NMETH1149

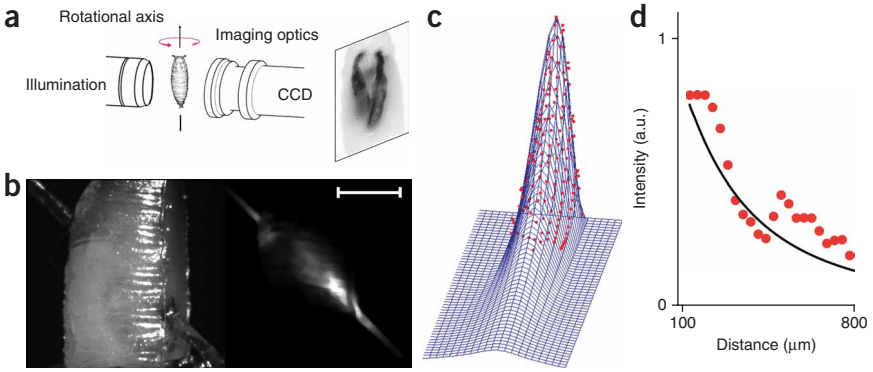

Figure 1 | Overview of the experimental configuration. (**a**) The microscope is horizontally mounted, and the sample lies vertically on a high-speed-rotation stage. A laser beam is focused by way of a low-numerical-aperture objective in close proximity to the center area of the pupa's surface. The sample is then rotated and images are captured with a CCD mounted on the microscope. (**b**) A flexible fused silica capillary tubing (Polymicro Technologies) with an external and internal diameter of 105 and 40 μm, respectively, was filled with a fluorescent dye (Cy5.5). The tubing penetrates from one side of the pupa and exits on the opposite side as shown in white light images (left) and fluorescence images (right); the projections are taken at two orthogonal angles. Scale bar, 500 μm. (**c**) Experimentally measured photon density propagation function for the pupa shown in **b** (filled red circles) and fitting Fermi function (blue mesh) for the central detector. The data demonstrate the presence of a strongly scattering forward component. (**d**) Plot of the experimental data (filled red circles) along the central axis of propagation, and fitting (black line) with the Fermi function.

populations (that is, abdominal histoblasts in the pupa[13]) combined with the use of GFP markers has allowed analysis of some processes over time, three-dimensional reconstruction of internal organs in living pupae has not been achieved. We discuss how the technique we developed can operate at varying degrees of photon scattering, and can be applied to different species and targets.

To enable experimental verification, we used an in-house built tomographic microscope (**Fig. 1a** and **Supplementary Fig. 1** online). Light from an argon ion continuous wave laser was beam expanded to fill the back aperture of a low-numerical-aperture objective before illuminating the sample under investigation. The light detection was based on a Leica microscope consisting of a Z16 APO apochromatically corrected zoom, combined with a 1× or 2× objective with 97 and 39 mm working distance, respectively, and focused on the sample. The microscope was horizontally mounted for the sample to lay vertically on a Newport PR50 high speed rotation stage. Light detection at the excitation and emission wavelengths was performed by a charge-coupled device (CCD) camera using narrow band-pass interference filters (excitation filter, 488 ± 5 nm; emission filter, 513 ± 5 nm). To improve image quality and reduce photon diffusion, we placed a polarization analyzer in front of the microscope and oriented it in parallel to the incident polarization light so as to reject highly scattered photons, that is, photons that loose their polarization state. A shutter, present on the beam pathway, avoided continuous illumination during the rotational scanning or when the sample was not imaged. This prevented damage from laser heat. A complete description of the setup is available in the **Supplementary Methods** online.

To confirm an appropriate mathematical (forward) model for reconstruction purposes, we inserted an 105 μm–diameter flexible fused silica capillary tubing filled with a Cy5.5 fluorescent dye in a wild-type *D. melanogaster* pupa (**Fig. 1b**) and imaged it over 360 projections at 10-degree steps. Then we measured the photon field received from each of the detectors as a response to the excitation light and the needle position in the three-dimensional space, and from these data calculated a two-dimensional map representing the relative sensitivity of each of the voxels in the *D. melanogaster* volume to the illumination field for each particular detector. The experimentally measured sensitivity function for the central detector (**Fig. 1c**) demonstrates the presence of a strong forward component in the scattering. Using the Fermi simplification of the Fokker Planck approximation, integrated over the physical area seen by each pixel on the CCD camera used, we were able to reasonably fit the experimental data (**Fig. 1d**) and to model the sensitivity of each detector (**Fig. 1c** and **Supplementary Methods**). For *in vivo* imaging, the pupae need to be monitored in the absence of any matching materials. This creates a refractive index mismatch between inner volume of the pupae and the surrounding air, which disturbs photon propagation resulting in

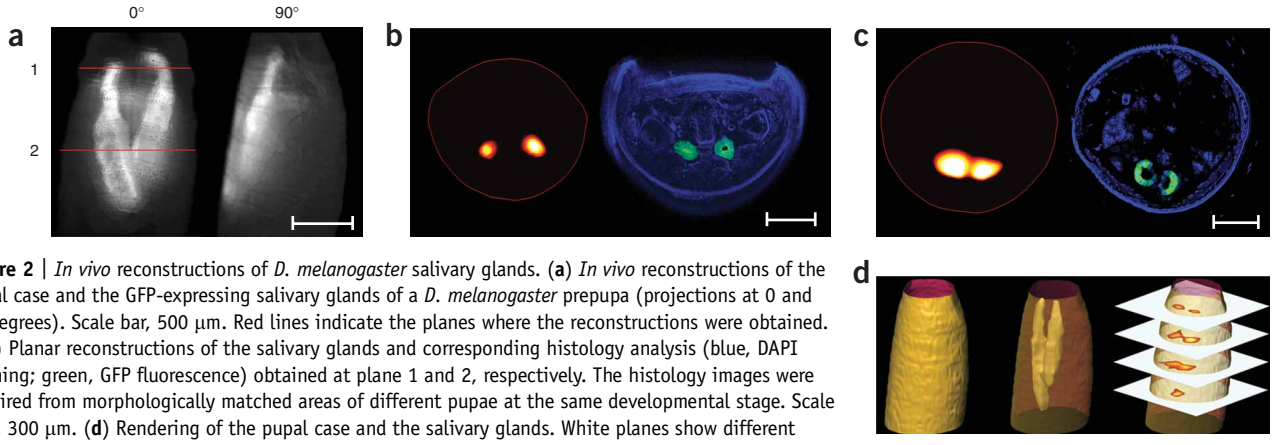

Figure 2 | *In vivo* reconstructions of *D. melanogaster* salivary glands. (**a**) *In vivo* reconstructions of the pupal case and the GFP-expressing salivary glands of a *D. melanogaster* prepupa (projections at 0 and 90 degrees). Scale bar, 500 μm. Red lines indicate the planes where the reconstructions were obtained. (**b**,**c**) Planar reconstructions of the salivary glands and corresponding histology analysis (blue, DAPI staining; green, GFP fluorescence) obtained at plane 1 and 2, respectively. The histology images were acquired from morphologically matched areas of different pupae at the same developmental stage. Scale bars, 300 μm. (**d**) Rendering of the pupal case and the salivary glands. White planes show different planar reconstructions obtained at different heights.

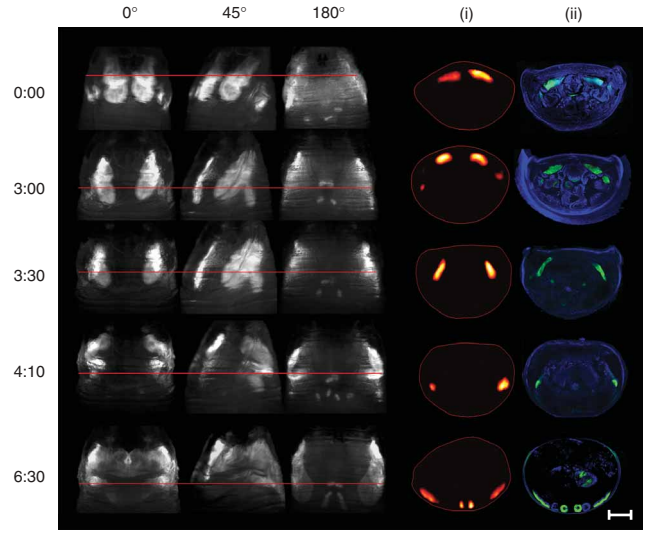

Figure 3 | Time-lapse imaging of *D. melanogaster* wing imaginal discs. The images were acquired from a single live specimen at five different time points (time indicated in h:min). Three different projections at 0, 45 and 180 degrees with respect to the pupa's dorsal view (anterior is up) are shown. The reconstructions in column i, correspond to the sections indicated by the red lines. Comparison with histology is shown in column ii. Histological preparations stained with DAPI correlate well with the reconstructions. The histological images were acquired from morphologically matched areas of different pupae staged accordingly. Scale bar, 300 μm.

lensing effects. Correspondingly, we corrected the application of the Fermi-based forward model by calculating the correct angle of propagation in the medium based on Snell's law of optical refraction.

We then imaged GFP-expressing salivary glands in three dimensions *in vivo* by illuminating the pupa with the excitation beam at powers below 7 mW; this cutoff guaranteed animal survival for at least 7 h of continuous imaging, with the pupae developing normally to healthy adult flies. We acquired fluorescence images (**Fig. 2a** and **Supplementary Videos 1–5** online) every 2 degrees in the range of 0–360 degrees, each using an exposure time of 1 s. It is also possible to use lower power or exposure time, by using CCD cameras with higher sensitivity. Reconstructed slices from measurements performed *in vivo* (**Fig. 2b–d**) had good congruence with corresponding histology data. We also investigated other reconstruction schemes (**Supplementary Fig. 2** online) and compared the resulting planar reconstructions with those obtained using the Fermi approximation. Corresponding histology analysis confirmed that only our method was capable of reconstructing the correct appearance of the salivary glands.

To interrogate whether longitudinal observations would be possible, we imaged morphogenetic movements that occur in the *D. melanogaster* pupae. In particular, using GFP expressed in the wing discs, we followed the morphogenesis of the wing and the thorax[14] during the first 6.5 h after pupariation. The time-lapse fluorescence imaging sequence (**Fig. 3**) shows the morphogenesis of the wing imaginal discs and is in good agreement with the corresponding histological sections. Composite image sequences acquired at different projections, showing the morphogenetic changes occurring in *D. melanogaster* pupae expressing GFP in the wing imaginal discs as a function of the time are shown in **Supplementary Videos 1–3**.

Studies to describe the development of small living organisms have largely relied on histological-section or whole-mount analysis of dissected tissues, making the processes time-consuming and requiring analysis of a large number of samples. Mesoscopic fluorescence tomography can allow rapid and continuous imaging of organism development, substantially accelerating procedures and can potentially be used to study mutations that affect development or responses to environmental conditions and administered chemicals. Although we imaged *D. melanogaster* pupal stages, potentially other stages or organisms can be studied as well by selecting mathematical models that more closely approximate the corresponding radiative transport equation. The method may offer a new dimension in biological research by seamlessly adding the time dimension to the observation and reveal not only the spatial but also temporal relationships of the various parameters associated with development, function and disease. Although we do not anticipate that mesoscopic imaging will be used as a stand-alone modality owing to the lower resolution achieved, it can be used in combination with standard *ex vivo* histological techniques to offer a complete picture of the underlying activity with mesoscopic resolution at the organism level and microscopic resolution at the cellular level. Future studies (**Supplementary Methods**) will aim to implement multispectral and fluorescence resonance energy transfer (FRET) tomographic imaging.

Note: Supplementary information is available on the Nature Methods website.

ACKNOWLEDGMENTS

We thank A. Soubret for his help and suggestions, and Polymicro Technologies LLC for providing us the fused silica capillary tubing. This work was supported by the US National Institutes of Health National Institute of Biomedical Imaging and Bioengineering grant RO1000750. C.P. is supported by an European Molecular Biology Organization fellowship. N.P. is a Howard Hughes Medical Institute investigator.

AUTHOR CONTRIBUTIONS

C.V. and C.P. designed the experiment. C.V. developed the system, performed the experiments, developed the image processing and inversion schemes, analyzed data and wrote most of the paper. C.P. generated the GFP-expressing flies and performed histology and confocal microscopy. D.R. developed the inversion schemes, image reconstruction software and contributed to developing the photon propagation model. N.P. and V.N. supervised the project.

Published online at http://www.nature.com/naturemethods/
Reprints and permissions information is available online at http://npg.nature.com/reprintsandpermissions

1. Helmchen, F. & Denk, W. *Nat. Methods* **2**, 932–940 (2005).
2. Yuste, R. *Nat. Methods* **2**, 902–904 (2005).
3. Minsky, M. US patent 3,013,467 (1961).
4. Huang, D. *et al. Science* **254**, 1178–1181 (1991).
5. Weissleder, R., Tung, C.H., Mahmood, U. & Bogdanov, A. *Nat. Biotechnol.* **17**, 375–378 (1999).
6. Ntziachristos, V., Ripoll, J., Wang, L.H.V. & Weissleder, R. *Nat. Biotechnol.* **23**, 313–320 (2005).
7. Arridge, S.R. *Inverse Probl.* **15**, R41–R93 (1999).
8. Sharpe, J. *et al. Science* **296**, 541–545 (2002).
9. Dodt, H.U. *et al. Nat. Methods* **4**, 331–336 (2007).
10. Pomraning, G.C. *Nucl. Sci. Eng.* **127**, 182–198 (1997).
11. Ward, R.E., Reid, P., Bashirullah, A., D'Avino, P.P. & Thummel, C.S. *Dev. Biol.* **256**, 389–402 (2003).
12. Sun, B., Xu, P. & Salvaterra, P.M. *Proc. Natl. Acad. Sci. USA* **96**, 10438–10443 (1999).
13. Ninov, N., Chiarelli, D.A. & Martin-Blanco, E. *Development* **134**, 367–379 (2007).
14. Zeitlinger, J. & Bohmann, D. *Development* **126**, 3947–3956 (1999).